Quantum phases in artificial molecules

Massimo Rontani[a,*], Filippo Troiani[a], Ulrich Hohenester[a,b], Elisa Molinari[a]

[a]*Istituto Nazionale per la Fisica della Materia (INFM) and Dipartimento di Fisica, Università degli Studi di Modena e Reggio Emilia, Via Campi 213/A, 41100 Modena, Italy*
[b]*Institut für Theoretische Physik, Karl-Franzens-Universität Graz, Universitätsplatz 5, 8010 Graz, Austria*

Abstract

The few-particle state of carriers confined in a quantum dot is controlled by the balance between their kinetic energy and their Coulomb correlation. In coupled quantum dots, both can be tuned by varying the inter-dot tunneling and interactions. Using a theoretical approach based on the diagonalization of the exact Hamiltonian, we show that the transitions between different quantum phases can be induced through the inter-dot coupling both for a system of few electrons (or holes) and for aggregates of electrons and holes. We discuss their manifestations, in addition energy spectra (accessible through capacitance or transport experiments) and optical spectra. © 2001 Elsevier Science Ltd. All rights reserved.

1. Introduction

Semiconductor quantum dots (QDs) are formidable laboratory materials for next-generation devices and for the actual realization of some key *Gedankenexperimente* in many-body physics [1–3]. Indeed, the number of electrons and holes in the QD can be controlled very accurately, and almost all relevant parameters influencing their strongly correlated states, like confinement potential and coupling with magnetic field and light, can be tailored in the experiments. The additional possibility of tuning the coupling between QDs enriches their physics and the possible applications.

From the point of view of fundamental physics, such coupling extends the analogy between quantum dots ('artificial atoms' [4]) and natural atoms, to artificial and natural molecules. The tunability of coupling among QDs allows to explore all regimes between non-interacting dots and their merging into a single QD; many of those regimes are precluded to molecular physics.

One of the peculiarities of QDs with respect to other solid state structures consists in the partial decoupling of a few degrees of freedom from all the others, which is due to the discrete nature of the spectrum [1–3]. The actual exploiting of such a feature largely depends on the capability of integrating arrays of QDs, thus increasing the number of degrees of freedom that one can address and coherently manipulate. This is precisely the strategy pursued by the semiconductor-based solid state implementations of quantum computation [5].

In general and basic terms, the tuning of inter-dot tunneling allows to modify the relative position of the single-particle levels, thus inducing phase transitions in the many-body ground states and different degrees of spatial correlation among carriers. Manifestations of these phenomena in systems formed by carriers of only one type, whose ground and excited state properties are accessible through addition energy spectra, have been predicted. Here we point out that similar effects are expected to occur also for systems formed by both electrons and holes. We also show that, in spite of the obvious differences, strong similarities appear in the analysis of electrons and electron–hole systems, and a unified theoretical description is in order. Basically, a competition emerges between two trends. On one side an atomic *Aufbau* logic, where carriers tend to occupy the lowest single-particle states available, thus minimizing the kinetic energy and the total spin, at the (energetic) cost of reducing spatial correlation among carriers. At the opposite extreme, we find an enhanced degree of spatial correlation among carriers, which occurs through the occupation of orbitals other than the lowest. This implies an enhancement of the kinetic energy and a reduction of the repulsive one,

* Corresponding author.
  E-mail addresses: rontani@unimo.it (M. Rontani), troiani@unimo.it (F. Troiani).

and results in electron distributions maximizing the total spin (Hund's rule). The balance between these two trends depends on the spacings of the single-particle levels involved, and these are precisely what can be settled by controlling the inter-dot tunneling. When carriers of opposite charge, different effective masses and tunneling parameters come into play, the competition between both trends becomes even more delicate.

Predictions of the actual ground and excited states of the many-body system thus require a careful theoretical treatment including all carrier–carrier interactions. Since the number of carriers in the dot can be controlled and kept relatively small, we can proceed through direct diagonalization of the exact many-body Hamiltonian, with no need to make a priori assumptions on the interactions. On the contrary, the results are a useful benchmark for the validity of the most common approximations for these systems.

We find that different quantum phases correspond to different regimes of inter-dot coupling both for a system of few electrons (or holes) and for aggregates of electrons and holes, with various possible spatial configurations and the formation of different possible 'subsystems' of inter-correlated particles. Besides, due to the negligible electron–hole exchange interaction in heterostructures such as GaAs, the two kinds of carriers can be treated as distinguishable particles. Therefore, spatial correlation among electrons and holes does not arise from the Fermi statistics: it needs instead the entanglement between the orbital degrees of freedom associated to holes and electrons, and turns out to depend only indirectly on the spin quantum numbers S_e and S_h.

After a brief summary of the state of the art in theoretical and experimental work on coupled dots (Section 2), in the following we describe the general Hamiltonian and solution scheme (Section 3). We then come to the results for electron- (Section 4) and electron–hole systems (Section 5). The trends leading to different quantum phases are discussed in detail, together with their nature in terms of spin and spatial correlation functions.

2. Experimental and theoretical background

Early experimental and theoretical studies focused on electrostatically coupled dots with negligible inter-dot tunneling [6]. Here we consider *artificial molecules* [7], where carriers tunnel at appreciable rates between dots, and the wavefunction extends across the entire system.

The formation of a miniband structure in a one-dimensional array of tunnel-coupled dots was demonstrated more than a decade ago [8]. After that, the first studies considered 'planar' coupled dots defined by electrodes in a two-dimensional electron gas. In these devices, the typical charging energy was much larger than the average inter-level spacing, hence linear [9–13] and non-linear [14] Single electron tunneling spectroscopy (SETS), obtained by transport measurements at different values of the inter-dot conductance, could be explained by model theories based on capacitance parameterizations [15–18]. Early studies also considered simple model Hamiltonians (usually Hubbard-like) with matrix elements treated as parameters [19–22]. Blick and coworkers clearly showed the occurrence of coherent molecular states across the entire two-dot setup, analyzing transport data [23,24] and the response to a coherent wave interferometer [25]. The tuning of coherent states was also probed by microwave excitations [26], and coupling with environment acoustic phonons was studied [27]. Planar coupled dots were also used to cool electron degrees of freedom [28], to measure the magnetization as a function of the magnetic field [29], and to study the phenomenon of 'bunching' of addition energies in large quantum dots [30]. The so-called 'vertical' experimental geometry was introduced later: it consists of a cylindrical mesa incorporating a triple barrier structure that defines two dots. So far, evidence of single-particle coherent states in a AlAs/GaAs heterostructure has been reported [31], while in AlGaAs/InGaAs structures clear SETS spectra of few-particle states have been observed as a function of the magnetic field B and of the inter-dot barrier thickness [32,33].

A relevant part of theoretical research has addressed the study of few-particle states in vertical geometries, within the framework of the envelope function approximation. The two-electron problem was solved, by means of exact diagonalization, in different geometries by Bryant [34] and by Oh et al. [35]. Systems with a number of electrons $N > 2$ at $B \approx 0$ in cylindrical geometry have been studied by several methods: Hartree–Fock [36], exact diagonalization for $N \leq 5$ [37,38], numerical solution of a generalized Hubbard Model for $N \leq 6$ [39,40] and for $N > 12$ with a 'core' approximation suitable for the weak-coupling regime only [41], density functional theory [42,43].

Palacios and Hawrylak [44] studied the energy spectrum in strong magnetic field and negligible inter-dot tunneling with various methods ($N \leq 6$), and established a connection between the correlated ground states of the double-dot system and those of Fractional Quantum Hall Effect systems in double layers. In this perspective, Hu et al. [45] studied collective modes in mean-field theory, Imamura et al. [46–48] exactly diagonalized the full Hamiltonian at strong B and different values of tunneling ($N \leq 4$), Martín-Moreno et al. [49] considered the occurrence of canted ground states. Also the far-infrared response of many-electron states was analyzed with various techniques [50,51]. Another interesting issue is the relation between quantum and 'classical' ground states [52] as the radius of the dot is enlarged, when electrons arrange to minimize electrostatic repulsion because the kinetic energy is quenched [53,54].

The electronic properties of planar dots have also been studied theoretically, through a variety of techniques: configuration interaction or analytical methods with various approximations [55–57], or density functional theory for larger values of N [58,59]. The infrared [60] and the
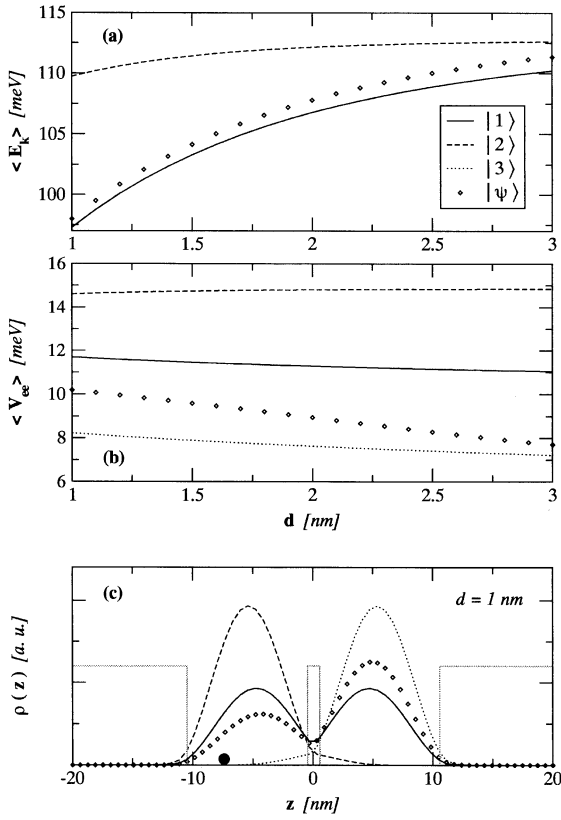
Fig. 1. Dependence on the inter-dot distance d of: (a) the kinetic $\langle E_k \rangle$ and (b) Coulomb $\langle V_{ee} \rangle$ energies of three prototypical two-electron states $|1\rangle \equiv |\sigma_g \uparrow, \sigma_g \downarrow\rangle$, $|2\rangle \equiv (|\sigma_g \uparrow, \sigma_u \downarrow\rangle - |\sigma_g \downarrow, \sigma_u \uparrow\rangle)/\sqrt{2}$ (singlet states) and $|3\rangle \equiv (|\sigma_g \uparrow, \sigma_u \downarrow\rangle + |\sigma_g \downarrow, \sigma_u \uparrow\rangle)/\sqrt{2}$ (triplet state); the symbol $\blacklozenge$ refers to the real ground state $|\psi\rangle$. In panel (c), we plot the spatially averaged pair-correlation function $\rho(z) \equiv \int \int P(x, y, z; x_0, y_0, z_0)\, dx\, dy$ corresponding to these states. The coordinates of the fixed particle (represented by the black circle) are $x_0 = 0$, $y_0 = 0$ and $z_0 = -7.5$ nm ($z = 0$ is in the middle of the inter-dot barrier). The continuous grey line gives the profile of the z component of the confinement potential (barrier height $V_0 = 400$ meV, in-plane confinement energy $\hbar\omega_0 = 20$ meV). Other parameters adopted are those typical of GaAs: $m_e^* = 0.067\, m_e$, $\kappa_r = 12.9$.

thermoelectric [61] response were considered. Systems of coupled QDs are also among the most promising candidates for the implementation of semiconductor-based quantum information processing devices: some of the current proposals identify the qubits with either the spin [62,63] or the orbital degrees of freedom associated to the conduction band electrons in QDs.

Research on few-electron systems in double dots is thus a new field in very rapid growth, with increasing focus on the possible quantum phases and how they can be driven by artificially controllable parameters such as inter-dot coupling, magnetic field, dot dimension. The study of such phases is expected to add insight into the physics of double

layers, e.g. the conditions for Wigner crystallization, and of strongly correlated systems in general. The amount of experimental data on many-body states in artificial molecules is still limited, but the whole bunch of spectroscopic tools currently available (linear and non-linear transport, Raman spectroscopy) is now beginning to be employed (see e.g. SETS spectra in the B–N space, Ref. [64] in this issue) and should allow the direct verification of theoretical predictions and a more general understanding of the basic phenomena and trends.

Also the optical properties of coupled QDs depend both on the confinement of electrons and holes and on the effects of correlation among these carriers. In spite of their importance, however, such correlation effects are still largely unknown. From the experimental point of view, cleaved-edge overgrown samples have been used [65], but self-organized quantum dots are most commonly employed for optics. Their stacking was demonstrated [66], and the splitting of the excitonic ground state in a single artificial molecule was studied as a function of the inter-dot distance. The lines in the photoluminescence spectra were explained in terms of transitions among excitonic states obtained by single-particle filling of delocalized bonding and anti-bonding electron and hole states [65,67]. When a few photoexcited particles are present, however, the correlations induced by the carrier–carrier Coulomb interactions play a crucial role;[1] single-particle tunneling and kinetic energies are also affected by the different energetic spacings of electron and hole single-particle states. The correlated ground and excited states will thus be governed by the competition of these effects, not included in previous theoretical descriptions of photoexcited artificial molecules [70]. A detailed understanding of exciton and multiexciton states in coupled semiconductor QDs, however, is of great interest for the development of the optical implementations of quantum-information processing schemes, starting from the identification of well characterized qubits [71]. The possibility of complete optical control over the computational space formed by interacting excitons in quantum dots has recently been demonstrated in Refs. [72,73]. We therefore expect that a systematic investigation of trends in the many-body phases of coupled dots will be actively pursued for systems of few electrons, and extended to systems of photoexcited electrons and holes in the near future.

3. Few-particle states of N electrons and holes

In the following, we focus on the motion of few electrons and holes confined in two coupled quantum dots. Our primary interest is in the correlated nature of ground and excited states of the interacting system.

---

[1] For single quantum dots it is now known from previous theoretical and experimental work that few-particle Coulomb correlations dominate the optical spectra in the non-linear regime. See, e.g. Refs. [68,69], and references therein.

Hereafter, we consider a simplified model where, within the envelope function and effective mass approximations, two coupled identical vertical dots are described by a separable confining potential $V(\rho, z) = V(\rho) + V(z)$, with $V(\rho) = 1/2(m^* \omega_0^2 \rho^2)$ an in-plane parabolic potential ($\vec{\rho} = (x, y)$, m^* is the effective electron (hole) mass, ω_0 the characteristic frequency) and $V(z)$ is a double square quantum well along the z direction (see Fig. 1). Each well (of width L and barrier potential height V_0) corresponds to a dot; the coupling between the two dots is controlled either by varying the inter-dot distance d (width of the inter-dot barrier) or the height of the inter-dot potential barrier. To vary d implies to consider differently grown devices. The full many-body Hamiltonian $\mathscr{H}$ (in zero magnetic field) is the sum of the single-particle terms $H^{(0)}(\vec{r}) = -\hbar^2 \nabla^2/(2m^*) + V(\rho, z)$ and of the two-body Coulomb interaction terms

$$\mathscr{H} = \sum_{\xi=e,h} \sum_{i=1}^{N_\xi} \left[H_\xi^{(0)}(\vec{r}_\xi^{(i)}) + \sum_{j<i} \frac{e^2}{\kappa_r |\vec{r}_\xi^{(i)} - \vec{r}_\xi^{(j)}|} \right]$$
$$- \sum_{i=1}^{N_e} \sum_{j=1}^{N_h} \frac{e^2}{|\vec{r}_e^{(i)} - \vec{r}_h^{(j)}|}. \tag{1}$$

Here κ_r is the dielectric constant of the semiconductor medium, and the subscript e (h) refers to electrons (holes). Effective masses, characteristic frequencies, and details of the double well entering $H^{(0)}$ differ for electrons and holes.

We chose this geometry for two reasons: firstly, experimental devices whose behavior can be described by this model are currently studied by several groups, allowing for precise tailoring of the dot geometry, strong spatial confinement, and hence observation of spectral features beyond the simple Coulomb Blockade behavior (e.g. in SETS spectra). Secondly, the cylindrical vertical geometry, contrary to in-plane devices, has the richest degree of symmetry, which is particularly helpful to theoretical work both in reducing the size of Hilbert space sectors and in analyzing electronic configurations. Specifically, $\mathscr{H}$ is invariant under any rotation in the spin space (the total spin S and its projection S_z are therefore conserved), rotation around the z-axis in real space (conservation of the z-component of the orbital angular momentum M), inversion with respect to the geometrical center of the system (parity conservation). In complete analogy with Molecular Physics [74] and for each species of carriers we introduce a spectroscopic notation to classify electronic terms, namely eigenstates of $\mathscr{H}$: $^{2S+1}M_{g,u}$. Here g (u) stands for even (odd) parity and M takes the labels $\Sigma, \Pi, \Delta, \ldots$ standing for $M = 0, 1, 2, \ldots$ Actually, a Σ term is also invariant under reflection with respect to a plane passing through the symmetry axis: in this case the notation takes the form $^{2S+1}\Sigma_{g,u}^{\pm}$, where $\pm$ labels the sign change under reflection.[2]

---

[2] The notation slightly differs from that used in Refs. [39,40], where $\pm$ refers to the reflection with respect to the xy plane. Ref. [49] defines this plane reflection as parity.

We are interested here in the evolution of the ground and excited states as the inter-dot distance d is varied. This feature shows a remarkable difference between artificial and natural molecules: in the latter the inter-nuclear distance is almost fixed, controlled by the nature of bonding, while in the former it can be tuned by adjusting electrodes or by growing different sample devices. Ground and excited states can be probed by several kinds of spectroscopies. Theoretically, once the energy spectrum is known after numerical diagonalization of $\mathscr{H}$, it is quite easy to compute the relevant observable quantities.

A considerable achievement has been obtained by transport spectroscopies, like single-electron capacitance tunneling spectroscopy [75] or SETS [76] for the ground state, or non-linear tunneling spectroscopy [77] for the excited states. In a transport experiment, the chemical potential $\mu(N)$ of the double-dot is measured as the number of electrons N is varied, charging the system one electron by one. In fact, from the experimental value $\mu(N)$ one can infer information about the ground state, being $\mu(N) = E_0(N) - E_0(N-1)$, with $E_0(N)$ the ground-state energy of the N-body system [78]. Our theoretical strategy is straightforward: we compute the ground state energies $E_0(N)$ at different values of N, and from these the chemical potential μ to be compared with the spectra. Single-dot far-infrared spectroscopies [1–3] are unsuitable to probe the relative motion of electrons and hence their correlation, because light only couples to the center-of-mass motion (generalized Kohn theorem) [79]. This is also true for a system of coupled identical quantum dots with cylindrical symmetry, as long as the in-plane confinement potential (orthogonal to the symmetry axis, e.g. the growth direction) is parabolic and the polarization of light is in the same plane. However, this limitation does not hold for two-photon processes like Raman scattering, where density fluctuations can excite collective modes of the interacting system [80,81].

Finally, optical spectroscopy allows the study of few-particle states including electrons and holes. In the lowest order, the light–semiconductor coupling is associated either to the absorption of a photon and to the promotion of an electron from the valence to the conduction band or to the reversed process, which is accounted for by a Hamiltonian of the form $-\mathbf{E} \cdot \mathbf{P}$, where $\mathbf{E}$ is the electric field and $\mathbf{P}$ the material polarization [82]. Within the rotating-wave and dipole approximations the luminescence spectrum for a QD initially prepared in state $|\lambda\rangle$ can be computed according to Fermi's golden rule

$$L_\sigma(\omega) \propto \sum_{\lambda'} |(P_\sigma)_{\lambda', \lambda}|^2 \delta(E_\lambda + \hbar\omega - E_{\lambda'}), \tag{2}$$

here $(P_\sigma)_{\lambda, \lambda'}$ are the dipole matrix elements corresponding to the transition between states λ and λ' (through removal of one electron–hole pair) and the creation of a photon with helicity $\sigma = \pm$.

4. Few-electron system

In this section, we study the system of interacting carriers of the same species, e.g. electrons. Let us start from the simplest case, that is the two-electron molecule. A theorem due to Wigner [83] guarantees that the ground state is always a singlet if time-reversal symmetry is preserved:[3] however, dramatic alterations of the energy spectrum and wavefunction are driven by the inter-dot distance d and the characteristic dot radius $\ell_0 = (\hbar/m^*\omega_0)^{1/2}$.

This is shown in Fig. 1: in panels (a) and (b) we plot the total ground state kinetic $\langle E_k \rangle$ and Coulomb $\langle V_{ee} \rangle$ energy,[4] respectively, vs d. Coulomb interaction mixes up different configurations (i.e. Slater determinants) which contribute with different weight to the ground state. Besides $\langle E_k \rangle$ and $\langle V_{ee} \rangle$ for the true few-particle groundstate $|\psi\rangle$ (symbol ◆), in Fig. 1 we also show the corresponding data of three proto-typical states:[5] $|1\rangle \equiv |\sigma_g \uparrow, \sigma_g \downarrow\rangle$ (singlet), $|2\rangle \equiv (|\sigma_g \uparrow, \sigma_u \downarrow\rangle - |\sigma_g \downarrow, \sigma_u \uparrow\rangle)/\sqrt{2}$ (singlet), $|3\rangle \equiv (|\sigma_g \uparrow, \sigma_u \downarrow\rangle + |\sigma_g \downarrow, \sigma_u \uparrow\rangle)/\sqrt{2}$ (triplet). Note that the difference between the (identical) kinetic energies of states $|2\rangle$ and $|3\rangle$ and that of $|1\rangle$ amounts exactly to the energy splitting Δ_{sas} between the single-particle states σ_u and σ_g (Fig. 1a). This quantity decreases exponentially as d increases and as the probability of the tunneling through the potential barrier goes to zero. While singlet and triplet states $|2\rangle$ and $|3\rangle$ have identical kinetic energy, the latter state is energetically favored as the interaction energy is concerned. The splitting in $\langle V_{ee} \rangle$ between $|2\rangle$ and $|3\rangle$ appearing in Fig. 1b is an *exchange energy*, namely the consequence of the antisymmetry of the total wavefunction for particle permutations. The behavior of the ground state $|\psi\rangle$ partly resembles that of the state $|1\rangle$, but shows significant deviations due to the mixing of configurations.

The arrangement of electrons is naturally visualized by computing density functions in real space. However, both the single-particle density and the usual radial pair correlation function $g(\rho)$ plotted in the xy plane depend only on the relative distance, due to the cylindrical symmetry of the system. Hence, we follow Ref. [85] and calculate the 'angu-lar' spin-resolved pair correlation function

$$P_{s,s_0}(\vec{\rho}, z; \vec{\rho}_0, z_0) = A_{s,s_0} \left\langle \sum_{i \neq j} \delta(\vec{\rho}^{(i)} - \vec{\rho})\delta(z^{(i)} - z) \right.$$
$$\left. \times \delta_{s^{(i)},s} \delta(\vec{\rho}^{(i)} - \vec{\rho}_0)\delta(z^{(j)} - z_0)\delta_{s^{(j)},s_0} \right\rangle, \quad (3)$$

where $\langle\cdots\rangle$ denotes the expectation value on a given state, the subscript s refers to spin, and A_{s,s_0} is a normalization factor, such that $\int d\vec{\rho}\, dz\, d\vec{\rho}_0\, dz_0 P_{s,s_0}(\vec{\rho}, z; \vec{\rho}_0, z_0) = 1$. One electron with spin s_0 is fixed at the position $(\vec{\rho}_0, z_0)$, while the other at $(\vec{\rho}, z)$ with spin s is varied: thus $P_{s,s_0}(\vec{\rho}, z; \vec{\rho}_0, z_0)$ is proportional to the conditional probability of finding the second electron given that the first one is fixed. This allows for observation of the relative spatial arrangement of electrons and of the angular correlation. The spin-independent quantity is the total pair correlation function $P(\vec{\rho}, z; \vec{\rho}_0, z_0)$, normalized as

$$P(\vec{\rho}, z; \vec{\rho}_0, z_0) = \frac{\left[\sum_{s=s_0} N_s(N_s - 1)P_{s,s_0} + \sum_{s \neq s_0} N_s N_{s_0} P_{s,s_0} \right]}{N(N-1)}, \quad (4)$$

N_s being the number of spin-s electrons.

In Fig. 1c, we plot the function $\rho(z) \equiv \int \int dx\, dy P(x, y, z; x_0, y_0, z_0)$, showing how the fixed position of one electron (represented by the black circle) affects the spatial distribution of the other one along the symmetry axis z, for an inter-dot distance of 1 nm. The state $|1\rangle$ clearly exhibits no spatial correlation among the two carriers: the placing of one electron in one quantum dot (QD) does not change the probability of finding the other one in any of the dots. In the case of the singlet state $|2\rangle$ the spatial distribution of one electron is peaked around the other (fixed) one: the two particles tend to occupy the same QD. Opposite trends apply to the triplet state $|3\rangle$. Again, the true ground state shows a mixed character: $\rho(z)$ has its biggest peak in the 'unoccupied' QD, but there is a finite probability for the double occupancy on the same QD. The average values of the Coulomb energy $\langle V_{ee} \rangle$ (Fig. 1b) clearly reflect such behaviors. The curve referring to $|1\rangle$ slowly decreases, because the value of $\langle V_{ee} \rangle$ corresponding to two particles in different QDs diminishes as d increases. A fortiori, $\langle V_{ee} \rangle$ decreases for the triplet state: the electrons are always in different QDs. The Coulomb energy is less affected by the inter-dot distance in the case of the state $|2\rangle$, because $\langle V_{ee} \rangle$ is mainly due to intra-dot interaction (both carriers in the same QD): the slight increase of $\langle V_{ee} \rangle$ depends on the growing localization of the particles within a QD.

The terms contributing to the Hamiltonian $\mathcal{H}$ of Eq. (1) scale differently with the characteristic length of the confinement potential ℓ_0: the kinetic one goes like $\sim \ell_0^{-2}$, while the interaction one like $\sim \ell_0^{-1}$. For small dots, the kinetic term dominates and the system is Fermi-

---

[3] The magnetic field breaks time-reversal symmetry and induces singlet–triplet transitions. In the artificial Helium this proceeds with increments of the quantum of angular momentum $\hbar$ (see Ref. [84]).

[4] Here by kinetic energy we mean the sum of the single-particle contributions to the total energy, thus including the effect of the external confinement potential.

[5] We describe a configuration listing the occupied single-particle levels, labeled as $nm_{g,u}^\pm$: n is the radial quantum number, m assumes the symbols $\sigma, \pi, \delta, \ldots$ corresponding to the azimuthal quantum number $m = 0, 1, 2, \ldots$, the superscript $+$ $(-)$ stands for positive (negative) values of m, and the subscript g (u) refers to even (odd) parity. Cf. Ref. [74].

singlet   triplet

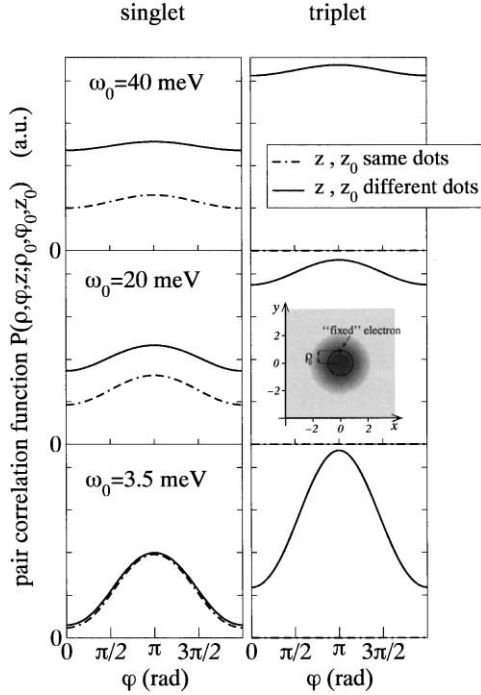

Fig. 2. Angular pair correlation function $P(\rho, \varphi, z; \rho_0, \varphi_0, z_0)$ vs the azimuthal angle φ for $N = 2$: all other parameters $\rho, \vec{\rho}_0, z, z_0$ are fixed, with $\rho = \rho_0$. Here ρ_0, z_0, z correspond to the average value of the in-plane radius and the maxima along z of the single-particle density, respectively. We use $m^* = 0.067m_e$, $\kappa_r = 12.9$, $L = 10$ nm, $V_0 = 400$ meV, $d = 1$ nm. The inset is a contour plot of $P(\vec{\rho}, z; \vec{\rho}_0, z_0)$ in the xy plane (in units of ℓ_0), for the triplet excited state with $\hbar\omega_0 = 20$ meV.

liquid like: here the ground state is determined by the successive filling of the empty lowest-energy single-particle levels, according to *Aufbau* atomic theory. As ℓ_0 increases, the electrons become more and more correlated and arrange to minimize Coulomb repulsion, up to the limit of complete spatial localization (reminiscent of Wigner crystallization in 2D). Even if for $N = 2$ the ground state is always a $^1\Sigma_g$ term as ℓ_0 is varied, nevertheless we can gain further insight into the correlation dynamics by analyzing the two-body wave-function.

In the inset of Fig. 2, we plot the total pair correlation function $P(\vec{\rho}, z; \vec{\rho}_0, z_0)$ for the $N = 2$ triplet state. Here, ρ_0 and z_0 are set equal to the average value of the in-plane radius and the maximum along z of the single-particle density, respectively. In addition, z is fixed at the position of the second, symmetric maximum of density in the symmetry-axis direction: the resulting contour plot is the value of P in the xy plane (in units of ℓ_0). This represents the probability of finding one electron in the plane of one dot, given that the second electron is fixed on the other dot. The other plots in Fig. 2 show $P(\rho, \varphi, z; \rho_0, \varphi_0, z_0)$ vs the azimuthal angle φ: all other parameters $\rho, \vec{\rho}_0, z, z_0$ are fixed, with $\rho = \rho_0$. When $\varphi = \varphi_0$, the position coincides

with that of the fixed electron, and the probability P has a minimum (zero in the triplet case with $z = z_0$) due to the Pauli exclusion principle. As φ is varied, the position follows a trajectory like the thick circle in the inset, starting from the bullet locating the other fixed electron in the xy plane. After a 2π-rotation, we are back in the starting point. These plots are a kind of 'snapshot' of the angular correlation, as we freeze the motion of one electron. Fig. 2 is organized into two columns, corresponding to the singlet ground state and to the triplet excited state, respectively, for different values of $\hbar\omega_0(d = 1$ nm$)$. Solid lines refers to the case $z = z_0$, namely electrons on the same dot, while dashed lines to $z \neq z_0$, i.e. electrons on different dots. When $\hbar\omega_0$ is very large (40 meV, top row), the curves $P(\vec{\rho}, z; \vec{\rho}_0, z_0)$ are almost flat. This flatness implies that the motion of the two electrons is substantially uncorrelated, except the effect of Fermi statistics. In fact, in the triplet case, the probability of measuring two electrons on the same dot is negligible, and this holds at any value of $\hbar\omega_0$. On the contrary, in the singlet state there is a finite probability of measuring two electrons on the same dot in the ground state. As $\hbar\omega_0$ is reduced (20 meV, middle row), angular correlation is turned on. This can be seen by the increase of the peak–valley ratio in the angular correlation function. The position of the maximum corresponds to π, i.e. the two electrons repelling each other tend to be separated as much as possible. This trend is even clearer at small values of $\hbar\omega_0$ (3.5 meV, bottom row). Plots of the second row ($\hbar\omega_0 = 20$ meV) should be compared with the corresponding plot of Fig. 1(c): the first ones illustrate how electrons correlate in the xy plane, the second one how they arrange along z.

Note that in the first column of Fig. 2 as $\hbar\omega_0$ is decreased the probability of measuring two electrons on the same dot increases up to the limit when it equals the probability of measuring electrons on different dots ($\hbar\omega_0 = 3.5$ meV). This is due to the different ratios between two fundamental energy scales: the harmonic oscillator inter-level separation $\hbar\omega_0$ and the energy difference Δ_{sas} between antisymmetric and symmetric double-well wavefunctions: if $\hbar\omega_0 \gg \Delta_{sas}$, the inter-dot tunneling is negligible with respect to the kinetic energy of the intra-dot motion, and the dots are almost quantum mechanically decoupled. In the opposite limit, the system is coherent, and it makes no difference between measuring one electron on one dot or on the other one, since the system behaves as a unique dot, doubled in size.

Let us now turn to discuss the case $N > 2$. We choose a particular set of parameters, namely $m^* = 0.067m_e$, $\kappa_r = 12.4$, $L = 12$ nm, $V_0 = 250$ meV, $\hbar\omega_0 = 5.78N^{-1/4}$, corresponding to a set of experimental devices currently under study [32,33]. The parameterization of $\hbar\omega_0(N)$ is meant to mimic the effect of the gate voltage on the electrostatic confinement potential $V(\rho)$ [42]. We exactly diagonalize the Hamiltonian $\mathscr{H}$ of Eq. (1) for $N \leq 6$, using up to 32 single-particle orbitals. The convergence is checked
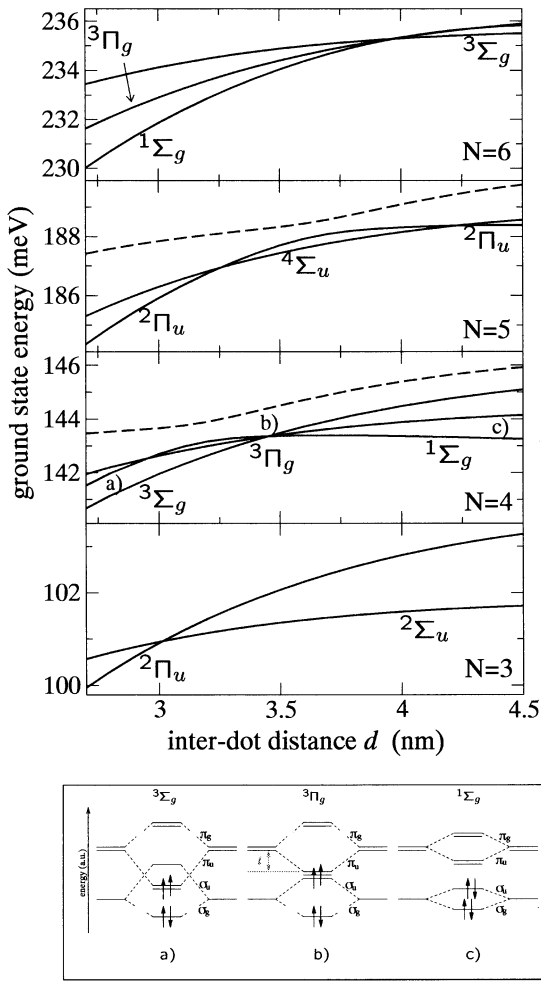
Fig. 3. Ground state energy vs d for different number of electrons. Some excited states are also depicted, together with their term in the Molecular Spectroscopy notation. The bottom panel pictorially shows the single-particle configurations that have the largest weight in the three different many-body ground states for $N = 4$.

controlling a cutoff on the average energy of the Slater determinants entering the computation. Our code uses the ARPACK package [86] and isolates Hilbert space sectors with S and S_z fixed, contrary to usual Lanczos approaches.

Fig. 3 shows the calculated ground state energy vs d for $3 \leq N \leq 6$. As d is varied, one or two transitions between ground states of different symmetries occur. Specifically, while there is only one transition between two different electronic terms for $N = 3$, two transitions take place for $N = 4$ and $N = 5$. The intermediate phase for $N = 4$ exists only in a very narrow range of d (~ 0.01 nm) in the neighborhood of $d = 3.45$ nm. For $N = 6$, again only two phases exist. However, at the intersection point of the $^1\Sigma_g$ and $^3\Sigma_g$ terms, the excited state $^3\Pi_g$ is almost degenerate in energy.

These transitions can be understood analyzing the many-body wavefunction of the different ground states [39,40]. In the bottom panel of Fig. 3 we focus on the $N = 4$ case and we schematically depict the major-weight Slater determinant corresponding to each phase. The key point is that, as d is decreased from the value of 4.5 nm, the 'energy-gap' Δ_{sas} between 'bonding' and 'anti-bonding' orbitals (i.e. symmetric and antisymmetric solutions of the double well along z) changes, from the limit of decoupled dots (labeled as (c) in figure) to the strong-coupling limit (labeled as (a)). In the (c) case, the first-shell molecular orbitals $0\sigma_g$ and $0\sigma_u$ are almost degenerate and well separated in energy with respect to the second shell, hence they are filled with four electrons giving the configuration $0\sigma_g^2 0\sigma_u^2$, i.e. two isolated dots with the first orbital shell completely filled. In the opposite limit, at small values of d ((a) case), the bonding mini-band made of $0\sigma_g$, $0\pi_u^+$, $0\pi_u^-$ single-particle orbitals is much lower in energy that the anti-bonding one. The ambiguity of how to fill the lowest-energy orbitals, due to the degeneracy of $0\pi_u^+$ and $0\pi_u^-$ levels, is solved consistently with Hund's first rule [76], i.e. the two open-shell electrons occupy each orbital with parallel spin (the configuration being $0\sigma_g^2 0\pi_u^+ 0\pi_u^-$), in such a way that exchange interaction prohibits electrons from getting close, minimizing Coulomb repulsion. This configuration is characteristic of a single dot, doubled in size [76]. In the intermediate phase (b), the antibonding $0\sigma_u$ level is almost degenerate with the bonding $0\pi_u^+$ and $0\pi_u^-$ levels: while the first two electrons occupy the lowest-energy orbital $0\sigma_g$, the remaining two arrange again to maximize spin, consistently to a 'generalized' Hund's first rule. However, now there are three levels almost degenerate, and we find that the ground state configuration is $0\sigma_g^2 0\sigma_u 0\pi_u^+$: according to Hund's second rule, also the total orbital angular momentum M is maximized, to minimize the interaction energy (the higher m, the smaller the Coulomb matrix element between single-particle levels). A similar reasoning applies to the transitions at $N \neq 4$.

Let us now focus on the $N = 5$ case in Fig. 3. As d increases, the ground state sequence is $^2\Pi_u \rightarrow {}^4\Sigma_u \rightarrow {}^2\Pi_u$, that is the $^2\Pi_u$ term appears twice, corresponding to a continuous energy curve that crosses twice the $^4\Sigma_u$ term. However, if we examine which Slater determinants mainly contribute to $^2\Pi_u$, we find that the relevant configuration at small d ($I \equiv 0\sigma_g^2 0\pi_u^{+2} 0\pi_u^-$) differs from that at large d ($II \equiv 0\sigma_g^2 0\sigma_u^2 0\pi_u^+$). Moreover, the slope of the curve in the two regions is different, mainly due to the change in the balance between bonding and anti-bonding levels occupied: 5:0 for I, 3:2 for II, which controls the dependence of the overall kinetic energy on d (see the previous discussion). This change in the 'character' of the $^2\Pi_u$ term (i.e. the ratio between the weights of configurations I and II) is found to be continuous with d. We plot also the first excited state for the $^2\Pi_u$ symmetry (dashed line in the $N = 5$ panel): clearly this curve anti-crosses the $^2\Pi_u$ ground state. Analyzing the slope and character of this excited state in the small- and large-d regions, we find an inverted behavior with respect to the ground state: now the relevant configuration
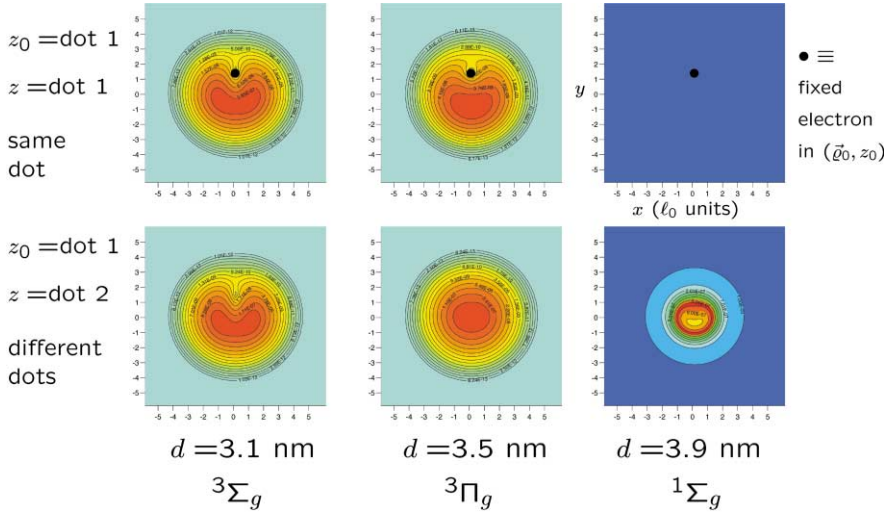
Fig. 4. Spin-resolved pair correlation function $P_{\uparrow,\uparrow}(\vec{\rho}, z; \vec{\rho}_0, z_0)$ for $N = 4$ for three different values of d (columns). The position of a spin-up electron $(\vec{\rho}_0, z_0)$ is fixed in one dot as in Fig. 2 (black bullet), and the contour plots of the top (bottom) row, with $z = z_0$ ($z \neq z_0$) fixed, correspond to the probability of measuring another spin-up electron on the same (other) dot in the xy plane (ℓ_0 units).

at small d is II while that at large d is I. The overall behavior can be understood as a consequence of the Wigner-von Neumann theorem, i.e. that intersection of terms of identical symmetry is forbidden [87]. Therefore, the two $^2\Pi_u$ terms anti-cross, while $^2\Pi_u$ and $^4\Sigma_u$ terms can freely cross and bring about ground state transitions, belonging to different irreducible representations of the symmetry group of $\mathscr{H}$. An analogous anti-crossing between ground and excited state for the $^1\Sigma_g$ symmetry is depicted in the $N = 4$ panel (solid and dashed line, respectively).

Results of Fig. 3 should be compared with those obtained by means of exact diagonalization of a generalized Hubbard model [39,40], by density functional theory [42,43], and by Hartree–Fock method [36]. In all these works, the window in d-space at which the ground state $^3\Pi_g$ at $N = 4$ occurs is much larger and a ghost additional intermediate phase at $N = 6$ (corresponding to the excited state $^3\Pi_g$ in our calculation) appears. Therefore our results, that agree well with data obtained up to $N \leq 5$ by exact diagonalization in Refs. [37,38], clearly demonstrate the importance of correlation beyond mean-field approaches. The interacting electronic system is so correlated in regimes of realistic parameters of the devices that it is very difficult to obtain quantitatively reliable results with any approach but configuration interaction. This point was already stressed, for single quantum dots, in Refs. [88,89].

To further characterize different ground states vs d, in Fig. 4 we plot the spin-resolved pair correlation function $P_{\uparrow,\uparrow}(\vec{\rho}, z; \vec{\rho}_0, z_0)$ for $N = 4$ for values of d corresponding to the three phases previously discussed. The position of a spin-up electron $(\vec{\rho}_0, z_0)$ is fixed in one dot as in Fig. 2, and the contour plots of the top (bottom) row, with $z = z_0$ ($z \neq z_0$) fixed, correspond to the probability of measuring another spin-up electron on the same (other) dot in the xy

plane. The right column refers to the $^1\Sigma_g$ term at $d = 3.9$ nm : there is only one 'free' spin-up electron, and we can see that the probability of measuring it on the same dot as the fixed electron is negligible, while the probability distribution on the other dot depends only slightly on the position of the first fixed electron. Therefore, the two dots are quantum mechanically decoupled, each one filled with two electrons in the lowest shell. The motion of electrons in the two dots is almost uncorrelated in the xy plane. In the opposite limit of small d (left column, $d = 3.1$ nm, three spin-up electrons), the coupling is so strong that it makes no difference either measuring the electron on one dot or on the other, i.e. the contour plots are identical, and the system forms a coherent, strongly bound molecule. The fixed electron is 'dressed' by its exchange and correlation hole, i.e. it repels other electrons that are at small distances. The middle column ($d = 3.5$ nm, three spin-up electrons) shows that in the intermediate phase $^3\Pi_g$ the dots are coupled with a weak degree of coherence, namely the probabilities of measuring the electron on the two dots are sensitively different. Planar correlation in the same dot is important, while it is negligible for motion on different dots. The above classification of phases is also suitable to $N \neq 4$.

In this section, we have shown results for the electron energy spectrum up to $N \leq 6$. It is straightforward now to compute the SETS linear spectrum, and comparison with very recent experimental data [64] shows remarkable agreement in many respects. Results for $B > 0$ will be presented elsewhere [90].

5. Few electron–hole pairs

We next consider systems of interacting carriers composed of an equal number of electrons and holes. Let
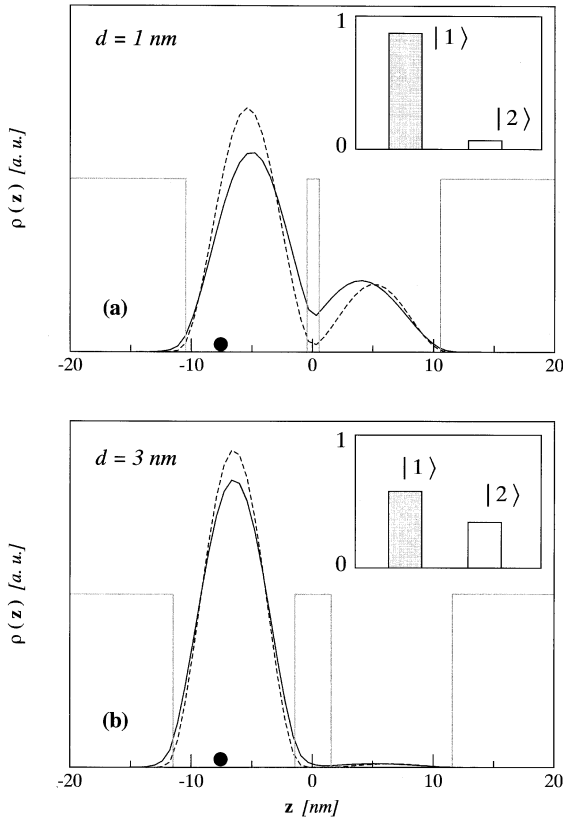
Fig. 5. Plot of the functions $\rho(z_e)$ (continuous line) and $\rho(z_h)$ (dashed line), computed for the excitonic ground states at $d = 1$ nm (a) and $d = 3$ nm (b). The definition of $\rho(z)$ and the positions of the fixed particles (either electron or hole) are as in Fig. 1. The columns in the insets represent the square moduli of the coefficients associated with the states $|1\rangle \equiv |\sigma_g^e \uparrow, \sigma_g^h \uparrow \rangle$ (grey column) and $|2\rangle \equiv |\sigma_u^e \uparrow, \sigma_u^h \uparrow \rangle$ (white column): the excitonic ground states are given, to a good degree of approximation, by the superposition of these two states. At $d = 1$ nm $|c_1|^2 = 0.871$ and $|c_2|^2 = 0.066$, while at $d = 3$ nm $|c_1|^2 = 0.577$ and $|c_2|^2 = 0.344$; minor contributions arise from occupations of higher-energetic single-particle states.

us start by considering a single electron–hole pair (exciton) and the way in which its ground state depends on the width of the barrier. As the inter-dot distance d increases, the splitting between the energies of the bonding (σ_g) and anti-bonding (σ_u) states decreases both for electrons and for holes. The energetic cost associated to the promotion of the two particles from the bonding to the anti-bonding states becomes smaller and comparable to the gain in Coulomb energy arising from the correlation of their spatial distributions along z. In Fig. 5 we plot the functions $\rho(z)$ of electrons and holes, associated to given positions of the other carrier, at inter-dot distances of $d = 1$ nm (a) and $d = 3$ nm (b); the two insets represent the contributions to the electron–hole ground states of $|1\rangle \equiv |\sigma_g^e \uparrow, \sigma_g^h \uparrow \rangle$ and $|2\rangle \equiv |\sigma_u^e \uparrow, \sigma_u^h \uparrow \rangle$. The decreasing tunneling goes with an increasing correlation (electron more localized around the hole and

vice versa) and an increasing contribution from the $|2\rangle$ state. The slight difference between the plots associated to electrons and holes at each inter-dot distance are due to the differences in the barrier heights (400 meV for electrons and 215 meV for holes) and in the effective masses ($m_e^* = 0.067m_0$ and $m_h^* = 0.38m_0$) of the two carriers: as a consequence electrons tunnel more than holes and tend to be less localized within one QD. It is worth noticing that at $d = 3$ nm, the electronic tunneling still induces a pronounced splitting between the two delocalized bonding and anti-bonding single-particle states ($\epsilon_b = 35.11$ meV and $\epsilon_a = 37.52$ meV). In spite of this, due to Coulomb correlation and to the reduced tunneling of holes, the energetic value and the spatial distribution of the excitonic ground state closely resembles that of an exciton in a single QD; besides, the splitting between the ground and the first excited states is negligible.[6] In other words the 'excitonic tunneling' is suppressed at smaller inter-dot distances than the electronic one.

If the double dot is occupied by two electrons and two holes, both attractive and repulsive interactions are present. Intuitively, one would expect carriers with identical charge to avoid each other and carriers of opposite charge to look for each other: the interplay between such trends is directed by the values of d and by those of S_e and S_h. In Fig. 6, we compare such correlations for two different values of the electron and hole spin quantum numbers and for $d = 1$ nm. The singlet–singlet lowest state ($S_e = 0$, $S_h = 0$) is characterized by a small correlation between the electrons, (a), and by a more pronounced one between holes, (c). Analyzing the eigenfunction associated to this state, one observes that approximately only the electron single-particle state σ_g^e is (twice) occupied, while for holes strong contributions arise from both bonding and anti-bonding states. As already mentioned, this difference between the behaviors of the two carriers depends on the fact that a gain in Coulomb energy has a greater kinetic cost for electrons than for holes. Besides, the spatial distribution of holes, (e), is not affected by the position of the electrons.[7] Let us now compare these correlation functions with the corresponding ones associated to the triplet–singlet configuration ($S_e = 1$, $S_h = 0$). Again the correlation among electrons and holes is negligible, (f): the two electrons and the two holes subsystems can thus be understood to a good extent independently from each other. As in the case of the prototypical state $|3\rangle$, that state of the two electrons here resembles, the probability of finding two electrons in

---

[6] The main contributions to the excitonic first excited state come from the states $|3\rangle \equiv |\sigma_g^e \uparrow, \sigma_u^h \uparrow \rangle$ and $|4\rangle \equiv |\sigma_u^e \uparrow, \sigma_g^h \uparrow \rangle$. At $d = 1$ nm $|c_3|^2 = 0.852$ and $|c_4|^2 = 0.0836$, while at $d = 3$ nm $|c_3|^2 = 0.348$, and $|c_4|^2 = 0.348$; in the latter case the correlation function looks very much like that of the ground state.

[7] Formally this means that the four-particle wavefunction can be written to a good degree of approximation in a factorized form: $\psi(\vec{r_{e1}}, \vec{r_{e2}}, \vec{r_{h1}}, \vec{r_{h2}}) \simeq \phi_e(\vec{r_{e1}}, \vec{r_{e2}})\phi_h(\vec{r_{h1}}, \vec{r_{h2}})$.

$S_e = 0$, $S_h = 0$ $S_e = 1$, $S_h = 0$ $S_e = 0$, $S_h = 0$ $S_e = 1$, $S_h = 0$
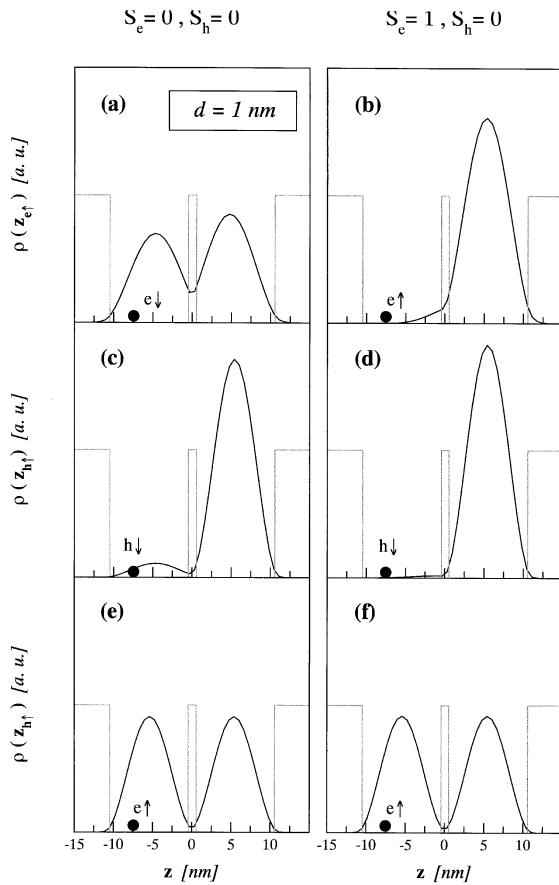

Fig. 6. The two spin configurations ($S_e = 0$, $S_h = 0$) and ($S_e = 1$, $S_h = 0$) are considered at $d = 1$ nm. The plots represent the spatial distribution of a carrier of spin orientation as specified by the subscript of the z-coordinate, given the position of another carrier is fixed (whose type and spin orientation are drawn close to the corresponding black circle). The position of the fixed particles is the one adopted in Fig. 1.

Fig. 7. Same functions as in Fig. 6, but for an inter-dot distance of 3 nm.

the same QD is negligible, (b). Such spatial separation of the electrons induces a more pronounced separation for the holes too, as shown by the flattening of the smallest peak in the left well (see Fig. 6b,d). The differences between the two spin configurations are even more dramatic at bigger inter-dot distances. In Fig. 7, we show the same correlation functions at $d = 3$ nm. The triplet–singlet configuration (Fig. 6b,d,f) shows the same features already observed at $d = 1$ nm; here the two electrons (holes) are perfectly localized in different QDs, due to the suppressed tunneling. The singlet–singlet configuration (Fig. 6a,c,e) instead has undergone a transition to a phase in which all carriers are localized in either QD (due to symmetry). If the position of one of the four particles is fixed in one QD, all the others are localized in the same one. This somehow surprising effect can be explained in the following way: in a mean field picture, due to the substantial similarity of the electron
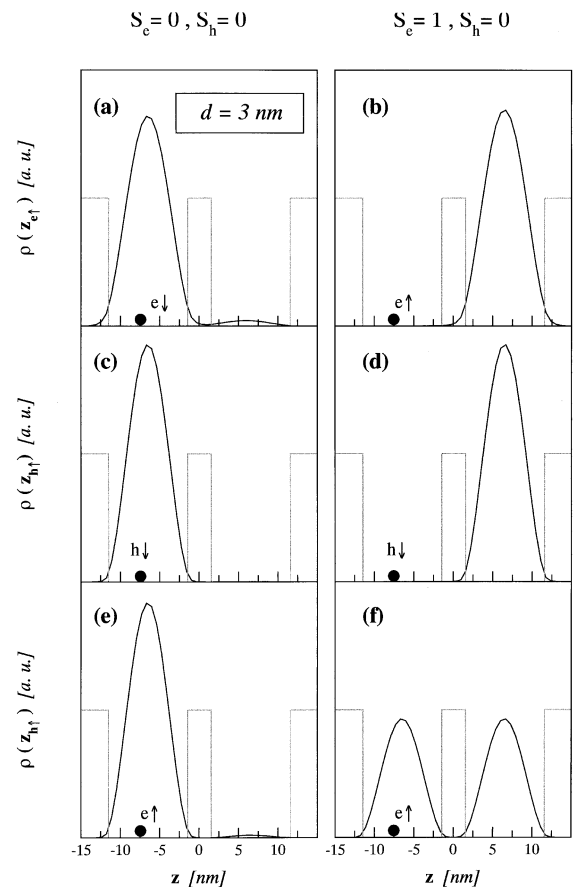
and hole wavefunctions, the localization of the two excitons in two different QDs or in the same one makes no difference with respect to the Coulomb energy because there is cancellation of terms of opposite sign. If correlation comes into play, however, the localization of all particles in the same QD gives rise to the so-called 'biexcitonic binding energy' ΔE (which is defined as the difference between twice the energy of the excitonic ground state and that of the biexcitonic one). Specifically, the binding energy ΔE is due to the correlations among the x and y directions: as in the case of the two electrons in Fig. 2, such correlations become strongly effective and lower the Coulomb energy when particles are localized in the same QD.

The comparison between the correlation functions corresponding to equal spin configurations at different inter-dot distances shows a trend similar to that of the two electrons alone. The population of the anti-bonding states increases with decreasing bonding–antibonding splitting, thus allowing a more pronounced spatial correlation between identical carriers. Such dependence is particularly clear for the singlet states, while for the triplet ones a high degree of correlation is already guaranteed by the permutational symmetry of the
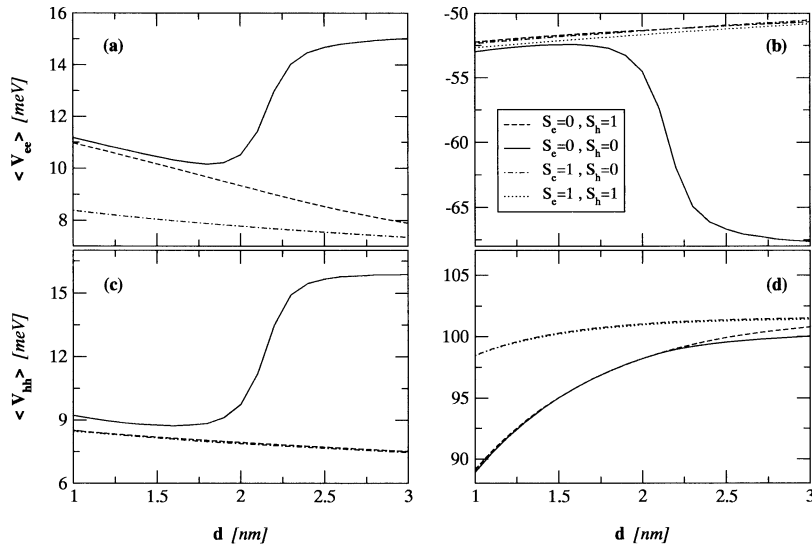
Fig. 8. Plots (a), (b) and (c) represent the d-dependence of the average values of the different contributions to the Coulomb energy for the eigenstates of lowest total energy associated to each of the four spin configurations (S_e, S_h). The curves associated to the (1,0) and (1,1) spin arrangements are identical in (a), and, together with (0,1), in (c). In (d) we plot the total energies.

few-particle wavefunction (i.e. by the fermionic nature of electrons and holes).

The described behaviors are reflected in the values of the different contributions to the mean Coulomb energies of each spin configuration (Fig. 8). Let us start by considering the three spin arrangements $(S_e, S_h) = (1, 1), (0, 1), (1, 0)$. The contributions to the Coulomb energy associated to the electron–electron interaction (a) all monotonically decrease with increasing d: the two electrons, each in a different QD, get more and more far apart. If $S_e = 1$ the spatial separation of the two electrons is a direct consequence of the permutational symmetry of the wavefunction; if $S_e = 0$ the same effect arises from a proper linear combination of different Slater determinants and from the corresponding occupation of the electronic σ_u^e orbitals (which in turn depends on the tunneling: from which the different slopes of the $S_e = 0$ and $S_e = 1$ curves). Analogous behaviors are seen to occur with respect to the hole–hole interaction (c). The main difference as compared to the previous case is the higher degree of correlation among such carriers in the $S_h = 0$ case, already at small inter-dot distances. The trends of the electron–hole Coulomb (b) interactions are hardly distinguishable one from the other. The monotonic decrease (in modulus) of $\langle V_{eh} \rangle$ reflects that of the interaction energy among carriers localized in different QDs when they get far apart. The plots associated to the singlet–singlet configuration (continuous lines), however, show a transition towards a phase in which all carriers are localized in a same QD, already put in evidence in Fig. 7. The absolute values of all Coulomb terms correspondingly go through an abrupt increase for values of d in the range between 2 and 2.5 nm. Let us finally consider the total energies (d). The lowest singlet–singlet

state turns out to be the system's ground state at any inter-dot distance. For $d \lesssim 2$ nm $S_e = 0$ and $S_e = 1$ configurations are degenerate with respect to the value of S_h; the difference between the total energies follows that between the two-electrons triplet and singlet states. As d increases, the energies of all spin configurations but $S_e = S_h = 0$ asymptotically tend to a value which is twice the energy of the excitonic ground state in a single QD. The energy of the singlet–singlet state instead tends to that of the biexcitonic ground state in a single QD: the difference between these two asymptotic values is the aforementioned biexcitonic binding energy ΔE.

6. Summary

We have presented a unified theoretical description of the correlated states of a few electrons (holes) or few excitons confined in coupled quantum dots. In these systems, interdot coupling controls the competition between kinetic energy and Coulomb interactions, and can reach regimes far out of those accessible in natural molecules. The resulting ground state is therefore very different for different values of the coupling: We have shown that a system of few electrons is characterized by different spin configurations depending on the inter-dot coupling, and we have extensively discussed the marked variations arising in the electron–electron correlation functions. In the case of two electrons and two holes we have identified the ground state corresponding to both pairs localized in one of the dots (weak coupling) or distributed in both dots (strong coupling). Tuning such phases by external fields is possible,

and is found to induce novel quantum effects that will be described elesewhere [90].

Manifestations of transitions between such phases in addition or optical spectra are expected to lead to a direct experimental verification of many-body-theory predictions, and to the experimental control of the few-particle states in nanoscale devices.

Acknowledgements

References

[1] L. Jacak, P. Hawrylak, A. Wójs, Quantum Dots, Springer, Berlin, 1998.

[2] D. Bimberg, M. Grundmann, N.N. Ledentsov, Quantum Dot Heterostructures, Wiley, Chichester, 1998.

[3] U. Woggon, Optical Properties of Semiconductor Quantum Dots, Springer, Berlin, 1997.

[4] M.A. Kastner, Phys. Today 46 (1993) 24.

[5] S. Lloyd, Science 261 (1993) 1569.

[6] For a review see: L.P. Kouwenhoven, C.M. Marcus, P.L. McEuen, S. Tarucha, R.M. Westervelt, N.S. Wingreen, in: L.L. Sohn, L.P. Kouwenhoven, G. Schoen (Eds.), Mesoscopic Electron Transport, Kluwer, Dordrecht, 1997, p. 105.

[7] L. Kouwenhoven, Science 268 (1995) 1440.

[8] L.P. Kouwenhoven, F.W.J. Hekking, B.J. van Wees, C.J.P.M. Harmans, C.E. Timmering, C.T. Foxon, Phys. Rev. Lett. 65 (1990) 361.

[9] F.R. Waugh, M.J. Berry, D.J. Mar, R.M. Westervelt, K.L. Campman, A.C. Gossard, Phys. Rev. Lett. 75 (1995) 705.

[10] F.R. Waugh, M.J. Berry, C.H. Crouch, C. Livermore, D.J. Mar, R.M. Westervelt, K.L. Campman, A.C. Gossard, Phys. Rev. B 53 (1996) 1413.

[11] C. Livermore, C.H. Crouch, R.M. Westervelt, K.L. Campman, A.C. Gossard, Science 274 (1996) 1332.

[12] T.H. Wang, S. Tarucha, Appl. Phys. Lett. 71 (1997) 2499.

[13] A.S. Adourian, C. Livermore, R.M. Westervelt, K.L. Campman, A.C. Gossard, Appl. Phys. Lett. 75 (1999) 424.

[14] C.H. Crouch, C. Livermore, R.M. Westervelt, K.L. Campman, A.C. Gossard, Appl. Phys. Lett. 71 (1997) 817.

[15] K.A. Matveev, L.I. Glazman, H.U. Baranger, Phys. Rev. B 53 (1996) 1034.

[16] K.A. Matveev, L.I. Glazman, H.U. Baranger, Phys. Rev. B 54 (1996) 5637.

[17] J.M. Golden, G.I. Halperin, Phys. Rev. B 53 (1996) 3893.

[18] J.M. Golden, G.I. Halperin, Phys. Rev. B 54 (1996) 16757.

[19] C.A. Stafford, S.D. Sarma, Phys. Rev. Lett. 72 (1994) 3590.

[20] G. Klimeck, G. Chen, S. Datta, Phys. Rev. B 50 (1994) 2316.

[21] G. Chen, G. Klimeck, S. Datta, G. Chen, W.A. Goddard III, Phys. Rev. B 50 (1994) 8035.

[22] R. Kotlyar, S.D. Sarma, Phys. Rev. B 56 (1997) 13235.

[23] R.H. Blick, R.J. Haug, J. Weis, D. Pfannkuche, K. von Klitzing, K. Eberl, Phys. Rev. B 53 (1996) 7899.

[24] R.H. Blick, D. Pfannkuche, R.J. Haug, K. von Klitzing, K. Eberl, Phys. Rev. Lett. 80 (1998) 4032.

[25] R.H. Blick, D.W. van der Weide, R.J. Haug, K. Eberl, Phys. Rev. Lett. 81 (1998) 689.

[26] T.H. Oosterkamp, T. Fujisawa, W.G. van der Wiel, K. Ishibashi, R.V. Hijman, S. Tarucha, L.P. Kouwenhoven, Nature (London) 395 (1998) 873.

[27] T. Fujisawa, T.H. Oosterkamp, W.G. van der Wiel, B.W. Broer, R. Aguado, S. Tarucha, L.P. Kouwenhoven, Science 282 (1998) 932.

[28] N.C. van der Vaart, S.F. Godijn, Y.V. Nazarov, C.J.P.M. Harmans, J.E. Mooij, L.W. Molenkamp, C.T. Foxon, Phys. Rev. Lett. 74 (1995) 4702.

[29] T.H. Oosterkamp, S.F. Godijn, M.J. Uilenreef, Y.V. Nazarov, N.C. van der Vaart, L.P. Kouwenhoven, Phys. Rev. Lett. 80 (1998) 4951.

[30] M. Brodsky, N.B. Zhitenev, R.C. Ashoori, L.N. Pfeiffer, K.W. West, Phys. Rev. Lett. 85 (2000) 2356.

[31] T. Schmidt, R.J. Haug, K. von Klitzing, A. Förster, H. Lüth, Phys. Rev. Lett. 78 (1997) 1544.

[32] D. Guy Austing, T. Honda, S. Tarucha, Jpn. J. Appl. Phys. 36 (1997) 1667.

[33] D.G. Austing, T. Honda, K. Muraki, Y. Tokura, S. Tarucha, Physica B 249-251 (1998) 206.

[34] G.W. Bryant, Phys. Rev. B 48 (1993) 8024.

[35] J.H. Oh, K.J. Chang, G. Ihm, S.J. Lee, Phys. Rev. B 53 (1996) R13264.

[36] H. Tamura, Physica B 249–251 (1998) 210.

[37] Y. Tokura, D.G. Austing, S. Tarucha, Proceedings of the 24th International Conference on the Physics of Semiconductors (World Scientific on CD-ROM, 1999), D. Gershoni (Ed.); Y. Tokura, D.G. Austing, S. Tarucha, J. Phys.: Condens. Matter 11 (1999) 6023.

[38] Y. Tokura, S. Sasaki, D.G. Austing, S. Tarucha, Physica E 6 (2000) 676.

[39] M. Rontani, F. Rossi, F. Manghi, E. Molinari, Solid State Commun. 112 (1999) 151.

[40] M. Rontani, F. Rossi, F. Manghi, E. Molinari, Mat. Res. Soc. Symp. Proc. 571 (2000) 179.

[41] Y. Asano, Phys. Rev. B 58 (1998) 1414.

[42] B. Partoens, F.M. Peeters, Phys. Rev. Lett. 84 (2000) 4433.

[43] M. Pi, A. Emperador, M. Barranco, F. Garcias, Phys. Rev. B 63 (2001) 115316.

[44] J.J. Palacios, P. Hawrylak, Phys. Rev. B 51 (1995) 1769.

[45] J. Hu, E. Dagotto, A.H. MacDonald, Phys. Rev. B 54 (1996) 8616.

[46] H. Imamura, P.A. Maksym, H. Aoki, Phys. Rev. B 53 (1996) 12613.

[47] H. Imamura, H. Aoki, P.A. Maksym, Phys. Rev. B 57 (1998) R4257.

[48] H. Imamura, P.A. Maksym, H. Aoki, Phys. Rev. B 59 (1999) 5817.

[49] L. Martín-Moreno, L. Brey, C. Tejedor, Phys. Rev. B 62 (2000) R10633.

[50] O. Mayrock, S.A. Mikhailov, T. Darnhofer, U. Rössler, Phys. Rev. B 56 (1997) 15760.

[51] B. Partoens, A. Matulis, F.M. Peeters, Phys. Rev. B 57 (1998) 13039.

[52] B. Partoens, V.A. Schweigert, F.M. Peeters, Phys. Rev. Lett. 79 (1997) 3990.

[53] C. Yannouleas, U. Landman, Phys. Rev. Lett. 82 (1999) 5325.

[54] B. Partoens, A. Matulis, F.M. Peeters, Phys. Rev. B 59 (1999) 1617.

[55] M. Eto, Solid-State Electron. 42 (1998) 1373.

[56] Yu.E. Lozovik, N.E. Kaputnika, Phys. Scripta 57 (1998) 542.

[57] N.E. Kaputnika, Yu.E. Lozovik, Fiz. Tverd. Tela 40 (1998) 2127 (Sov. Phys. Solid State, 40 (1998) 1929).

[58] S. Nagaraja, J.-P. Leburton, R.M. Martin, Phys. Rev. B 60 (1999) 8759.

[59] A. Wensauer, O. Steffens, M. Suhrke, U. Rössler, Phys. Rev. B 62 (2000) 2605.

[60] T. Chakraborty, V. Halonen, P. Pietiläinen, Phys. Rev. B 43 (1991) 14289.

[61] X. Chen, H. Buhmann, L.W. Molenkamp, Phys. Rev. B 61 (2000) 16801.

[62] G. Burkard, D. Loss, D.P. DiVincenzo, Phys. Rev. B 59 (1999) 2070.

[63] X. Hu, S.D. Sarma, Phys. Rev. A 61 (2000) 62301.

[64] S. Amaha, D.G. Austing, Y. Tokura, K. Muraki, K. Ono, S. Tarucha, Solid State Commun. 119 (2–3) (2001).

[65] G. Schedelbeck, W. Wegscheider, M. Bichler, G. Abstreiter, Science 278 (1997) 1792.

[66] S. Fafard, M. Spanner, J.P. McCaffrey, Z.R. Wasilewski, Appl. Phys. Lett. 75 (2000) 2268 and references therein.

[67] M. Bayer, P. Hawrylak, K. Hinzer, S. Fafard, M. Korkusinski, Z.R. Wasilewski, O. Stern, A. Forchel, Science 291 (2001) 451.

[68] A. Hartmann, Y. Ducommun, E. Kapon, U. Hohenester, E. Molinari, Phys. Rev. Lett. 84 (2000) 5648.

[69] A. Zrenner, J. Chem. Phys. 112 (2000) 7790.

[70] F. Troiani, U. Hohenester, E. Molinari, unpublished.

[71] C.H. Bennet, D.P. DiVincenzo, Nature (London) 404 (2000) 247.

[72] F. Troiani, U. Hohenester, E. Molinari, Phys. Rev. B 62 (2000) R2263 and references therein.

[73] E. Biolatti, R.C. Iotti, P. Zanardi, F. Rossi, Phys. Rev. Lett. 85 (2000) 5647.

[74] J.C. Slater, Quantum Theory of Molecules and Solids, Vol. 1, McGraw-Hill, New York, 1963.

[75] R.C. Ashoori, Nature (London) 379 (1996) 413.

[76] S. Tarucha, D.G. Austing, T. Honda, R.J. van der Hage, L.P. Kouwenhoven, Phys. Rev. Lett. 77 (1996) 3613.

[77] L.P. Kouwenhoven, T.H. Oosterkamp, M.W.S. Danoesastro, M. Eto, D.G. Austing, T. Honda, S. Tarucha, Science 278 (1997) 1788.

[78] C.W.J. Beenakker, Phys. Rev. B 44 (1991) 1646.

[79] W. Kohn, Phys. Rev. 123 (1961) 1242.

[80] D.J. Lockwood, P. Hawrylak, P.D. Wang, C.M. Sotomayor Torres, A. Pinczuk, B.S. Dennis, Phys. Rev. Lett. 77 (1996) 354.

[81] C. Schüller, K. Keller, G. Biese, E. Ulrichs, L. Rolf, C. Steinebach, D. Heitmann, K. Eberl, Phys. Rev. Lett. 80 (1998) 2673.

[82] H. Haug, S.W. Koch, Quantum Theory of the Optical and Electronic Properties of Semiconductors, World Scientific, Singapore, 1993.

[83] D.C. Mattis, The Theory of Magnetism, Harper, New York, 1965, p. 91.

[84] M. Wagner, U. Merkt, A.V. Chaplik, Phys. Rev. B 45 (1992) 1951.

[85] P.A. Maksym, Phys. Rev. B 53 (1996) 10871.

[86] R.B. Lehoucq, K. Maschhoff, D.C. Sorensen, C. Yang, ARPACK computer code, http://www.caam.rice.edu/software/ARPACK/

[87] L.D. Landau, E.M. Lifshitz, Quantum Mechanics — Non Relativistic Theory, Pergamon Press, Oxford, 1958.

[88] D. Pfannkuche, V. Gudmundsson, P.A. Maksym, Phys. Rev. B 47 (1993) 2244.

[89] M. Rontani, F. Rossi, F. Manghi, E. Molinari, Phys. Rev. B 59 (1999) 10165.

[90] M. Rontani, G. Goldoni, F. Manghi, E. Molinari, unpublished.